The Effect of Different Implementations of the Weak Temperature Gradient Approximation in Cloud Resolving Models

N. Z. Wong[1], **Z. Kuang**[1,2]

[1]Department of Earth and Planetary Sciences, Harvard University, Cambridge, MA, USA
[2]John A. Paulson School of Engineering and Applied Sciences, Harvard University, Cambridge, MA, USA

Key Points:

- Different implementations of the Weak Temperature Gradient result in divergent model behavior in idealized setups
- Divergent model behavior is caused by different treatment of baroclinic modes

Corresponding author: Nathanael Wong, `nathanaelwong@fas.harvard.edu`

Abstract

The Weak Temperature Gradient (WTG) approximation is a popular method used to couple convection in limited-area domain simulations with large-scale dynamics. However, several different schemes have been created to implement this approximation, and these different WTG schemes show a wide range of different results in an idealized framework. Our investigation shows that different model behavior is caused by the treatment of the different baroclinic modes by the different WTG schemes. More specifically, we hypothesize that the relative strengths of the baroclinic modes plays a large role in these differences, and show that modifying these schemes such that they treat the baroclinic modes in a similar manner accounts for many of the significant differences observed.

Plain Language Summary

The Weak Temperature Gradient (WTG) approximation uses the fact that temperature gradients are weak in the tropics to simplify the interaction in the tropics between local convection and the broader-scale tropical circulation. Several different schemes were created over the years to implement this approximation, and while they are broadly similar in many aspects, they also differ in the details. Although some previous studies aimed to quantify the differences between the implementations in various models, they did not delve into the reason behind these differences.

We investigated the different model behaviors that result when different WTG schemes are utilized in an idealized model setup. We show through both mathematical analysis of the relevant equations and model runs implementing these different WTG schemes, that the resultant model behavior is dependent on how higher-order baroclinic modes respond to temperature and buoyancy perturbations in the different WTG schemes. If we modify these schemes so that the strength of the response of higher-order baroclinic modes is similar, many of these differences in model behavior observed will be reduced.

1 Introduction

The Weak Temperature Gradient (WTG) approximation (Sobel & Bretherton, 2000) is a simplified framework for atmospheric dynamics in the deep tropics where the Coriolis force is weak. In such a framework, buoyancy gradients in the free troposphere are rapidly smoothed out by gravity waves, and thus spatial temperature gradients in the free troposphere are small. Local perturbations in buoyancy caused by heating (cooling) are assumed to be balanced by vertical ascent (subsidence). Thus, vertical motion is strongly coupled to convection within the deep tropics, as opposed to it being a one-way, causal, relationship (Raymond & Zeng, 2005). The WTG approximation is therefore a more suitable framework for parameterizing the large-scale circulation in the tropics as opposed to directly specifying the large-scale vertical ascent.

A number of studies (e.g., Raymond & Zeng, 2005; Sobel et al., 2007; Sessions et al., 2010; Daleu et al., 2012; Emanuel et al., 2014; Daleu et al., 2015, and others) have investigated the WTG approximation framework in small-domain Radiative-Convective Equilibrium (RCE) simulations. One common feature found in these studies is that applying the WTG approximation can cause a bifurcation in model equilibrium, resulting in either: (1) dry, often non-precipitating states, or (2) heavily-precipitating states. Emanuel et al. (2014) in particular deduced that these two regimes are analogues to the dry and wet regimes of self-aggregation seen in large-domain RCE simulations (Fig. 1a).

By design, the WTG approximation relaxes the model domain mean temperature profile toward an externally specified reference profile. In the work presented here, the reference profile is taken to be the radiative-convective equilibrium (RCE) profile produced by the model itself, similar to previous studies (e.g. Sessions et al., 2010; Emanuel

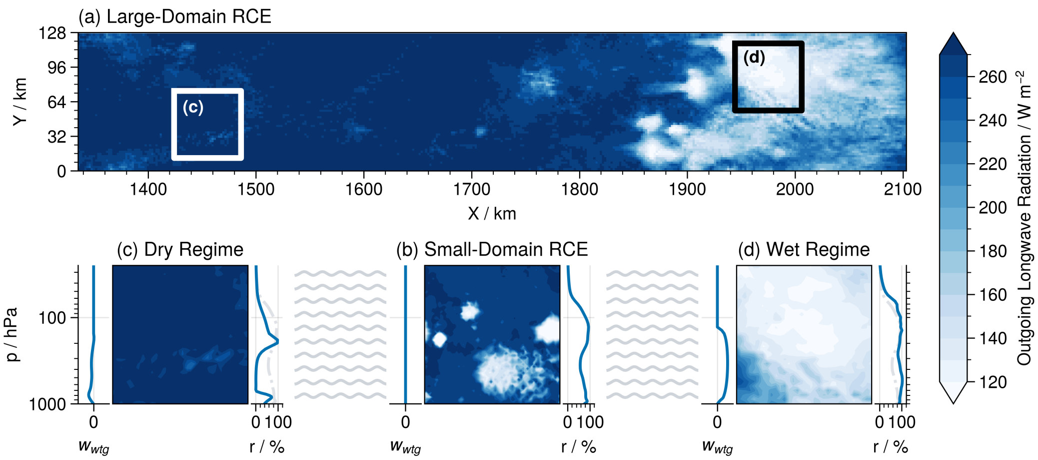

Figure 1. When (a) a large-domain simulation is run to RCE, the induced large-scale circulation causes self-aggregation of convection, resulting in the formation of (c) a dry, weakly/no-precipitating regimes with vertical subsidence and (d) moist, strongly precipitating regimes with vertical ascent. In (b) small-domain RCE runs, self-aggregation does not naturally occur, but previous studies have shown that implementations of the WTG approximation that parameterize the large-scale tropical circulation allow us to attain either of these two regimes. Here, w_{wtg} and r denote the domain-mean large-scale vertical velocity and relative humidity respectively.

et al., 2014). If this state is stable with WTG, applying the WTG framework will cause the model to converge to it, given the right initial conditions. However, if the RCE state is unstable with WTG, deviations can be expected to occur under the WTG framework, either in the form of the abovementioned bifurcation of the resulting model states in the previous paragraph, or in some form of oscillatory behavior if no stable state exists.

Over time, three main schemes that implement the WTG approximation in models have emerged: the (1) Temperature Gradient Relaxation (TGR) implementation (Raymond & Zeng, 2005), the (2) Damped Gravity Wave (DGW) implementation (Kuang, 2008a; Blossey et al., 2009), and the (3) Spectral (SPC) Weak Temperature Gradient implementation (Herman & Raymond, 2014). We provide more elaboration on these schemes in Section 2. Despite the prevalence of these schemes in modelling work for tropical climate, they often produce noticeably different results. For example, several studies (e.g. Romps, 2012b, 2012a; Daleu et al., 2015) show that the TGR implementation results in a vertical profile that is more top-heavy than the DGW implementation (Fig. S1).

Our study builds upon previous work done to quantify these discrepancies in model results (e.g. Daleu et al., 2015) by attempting to understand why they arise in the first place. In Section 2 we will discuss these three main implementations of the WTG approximation in models, explain how we implement them in Section 3 and then show in Section 4 that these schemes give markedly different results even in idealized setups. In Section 5, we perform a vertical-mode decomposition of the WTG schemes, and discuss our results in the framework of Gross Moist Stability in Section 6.

2 Weak Temperature Gradient Implementations in Models

There are three major schemes enforcing the WTG approximation that are widely used in single-column and small-domain cloud resolving modes.

2.1 The Temperature Gradient Relaxation Implementation

The TGR implementation directly links local buoyancy anomalies to large-scale vertical motion. Differences in buoyancy between the single-column or small-domain cloud-resolving model and the large-scale environment over a time-scale τ are balanced by the vertical advection of potential temperature $w\partial_z\theta$, such that at a height z_i in the free troposphere the WTG-induced vertical velocity w_{wtg} is given by:

$$w_{\text{wtg}}(z_i)\left.\frac{\partial\overline{\theta}}{\partial z}\right|_{z=z_i} = \frac{\overline{\theta}(z_i)-\theta_0(z_i)}{\tau}\cdot\sin\frac{\pi z}{z_t} \tag{1}$$

where z_t is the height of the tropopause, θ is the model potential temperature and θ_0 is the reference large-scale potential temperature. $\overline{(\cdot)}$ represents the domain-average of the variable $(\cdot)$. This implementation was first done by Raymond and Zeng (2005), and has been used in a number of other studies (e.g. Sessions et al., 2010; Daleu et al., 2012). In contrast to Raymond and Zeng (2005) who fixed $z_t = 15$ km, in our runs we allowed z_t to vary by setting it to be the level of the cold-point tropopause. We decided to let this level fluctuate over time for two reasons: (1) for consistency in our comparison with the setup of Blossey et al. (2009), and (2) the mean-state tropopause height in our experimental runs can change depending on the mean-state of the model when the WTG approximation is enforced - a model in a moist, highly-precipitating state will have a higher tropopause height compared to a model in a dry, non-precipitating state (Fig. S1). To prevent unrealistically large values of w_{wtg}, we set a lower-bound on static stability, $(\partial\overline{\theta}/\partial z)_{\text{min}} = 1$ K km^{-1}, similar to what is done in Raymond and Zeng (2005).

2.2 The Damped Gravity Wave Implementation

In contrast to the TGR implementation, the link between buoyancy and temperature anomalies to large-scale vertical motion in the DGW implementation is derived from the damping of gravity wave perturbations in the momentum equations (without Coriolis force) using a Rayleigh damping coefficient a_m:

$$u'_t = -\frac{1}{\rho}p'_x - a_m u' \tag{2}$$

$$v'_t = -\frac{1}{\rho}p'_y - a_m v' \tag{3}$$

where the other variables have their usual meteorological meaning. $(\cdot)'$ represents the perturbation of the variable $(\cdot)$ from the large-scale reference profile. Assuming (1) steady state, (2) that a_m is constant with height, and (3) using the ideal gas, hydrostatic balance and mass conservation laws, the momentum equations are transformed into the following governing equation for WTG-induced pressure velocity ω_{wtg} in pressure-coordinates:

$$\frac{\partial^2\omega'}{\partial p^2} = \frac{k^2}{a_m}\frac{R_d T'_v}{\overline{p}} \tag{4}$$

where R_d is the dry gas constant, T_v is the virtual temperature, and k is the horizontal wavenumber of the gravity wave. As mentioned above, $\overline{(\cdot)}$ and $(\cdot)'$ respectively denote the domain average of $(\cdot)$ and its perturbation from the large-scale reference profile. The strength of the implementation is controlled by k^2/a_m. As varying either will change model behavior in a similar manner, we keep $k = 2\pi/\lambda$ constant, taking $\lambda =$

2600 km and $a_m = 1$ day^{-1} as in Blossey et al. (2009), and multiply k^2/a_m by a dimensionless constant α.

Kuang (2008a) also derived a similar form using height coordinates instead of pressure coordinates. However, we used Eq. 4 to maintain consistency with Blossey et al. (2009). Furthermore, while we used virtual temperature T_v to be consistent with previous studies (e.g. Blossey et al., 2009), we have also verified by replacing T_v with absolute temperature T that the virtual effect does not contribute significantly to the differences we see across the different implementations.

2.3 The Spectral Weak Temperature Gradient

Herman and Raymond (2014) published an updated version of the TGR implementation of Raymond and Zeng (2005). Instead of assuming that gravity waves of all vertical wavelengths are equally effective in redistributing buoyancy/temperature anomalies, the relaxation time τ_j for the j-th vertical mode is $\tau_j = j \cdot \tau$, where τ is the relaxation timescale of the 1st vertical mode. Therefore, we perform a vertical decomposition of both vertical velocity and scaled potential temperature anomaly as follows:

$$w' = \sum_{j=1}^{n} w_j G_j(z) \qquad \frac{\theta'}{\partial_z \overline{\theta}} = \sum_{j=1}^{n} \theta_j G_j(z) \tag{5}$$

where the vertical modes are of the form:

$$G_j(z) = \frac{\pi}{2} \sin\left(\frac{j\pi z}{z_t}\right) \tag{6}$$

where similar to the TGR implementation as above, we decided to let z_t fluctuate over time. The Spectral Weak Temperature Gradient implementation then assumes that strength of the vertical mode of vertical velocity as a function of the vertical mode of the scaled potential temperature anomaly is given by $w_j = \theta_j/\tau_j$, such that the spectral WTG vertical velocity is given by

$$w' = \sum_{j=1}^{n} w_j G_j(z) = \sum_{j=1}^{n} \frac{\theta_j}{\tau_j} G_j(z) = \sum_{j=1}^{n} \frac{\theta_j}{j \cdot \tau} G_j(z) \tag{7}$$

We take $n = 32$ and neglect higher-order modes as importance decreases as the order increases.

3 Experimental Setup

3.1 Model Description

We used the System for Atmospheric Modelling (SAM) (Khairoutdinov & Randall, 2003) version 6.11.8. The model solves the anelastic continuity, momentum, and tracer conservation equations, with total nonprecipitating water (vapor, cloud water, cloud ice) and total precipitating water (rain, snow, graupel) included as prognostic thermodynamic variables. Simulations are run in three dimensions with doubly-periodic boundaries and a horizontal resolution at 2 km to permit clouds, with a horizontal domain of 128 km by 128 km. There are 64 vertical levels in our model, with the vertical spacing increasing from 50 m at the boundary layer to around 500 m at the tropical tropopause, to a total height of $\sim$27 km with a rigid upper-bound. Damping is applied to the upper third of the model domain to reduce reflection of gravity waves. A simple Smagorinsky-type scheme is used for the effect of subgrid-scale motion.

In all our experiments, the SST is fixed at 300 K, spatially uniform and time-invariant. We run two versions of the model: (1) the default version of SAM with the RRTM radiative scheme (Mlawer et al., 1997)), and (2) the idealized radiative scheme of Pauluis and Garner (2006) that uses a fixed radiative-cooling rate of -1.5 K day^{-1} in the troposphere and Newtonian relaxation when the temperature is less than 205 K with a relaxation timescale of 5 days.

3.2 Obtaining the Large-Scale Reference Profiles for WTG Simulations

As mentioned in Section 1, all simulations involving the WTG approximation require coupling of the model to a large-scale profile of the relevant buoyancy-variable (for e.g. in the DGW implementation (Eq. 5) this would be virtual temperature T_v). These reference profiles were obtained by spinning a 10-member ensemble to RCE over 2000 days, taking the last 500 days for statistics, with separate profiles constructed for full-radiation and idealized-radiation simulations. We then take the average of the vertical profiles of temperature and specific humidity of these ensemble members to construct the large-scale reference profiles.

When each model run is initialized, SAM reads in a sounding file containing vertical heights, pressure levels, and the profiles of potential temperature and specific humidity in order to construct the initial state of the atmosphere. If the profile is close to RCE that is in balance with the time-invariant SST, then the state of the equilibrated atmosphere after 1000 days should be close to the initial profile. We reinitialize the model with the equilibrated sounding profiles of temperature and specific humidity from our 10-member ensemble run and repeat this cycle until the root-mean-squared difference between the initial and final ensemble-mean temperature profiles was < 0.01 K.

3.3 Implementing the different schemes into SAM

Once the models have been spun-up to RCE, we take the average temperature and humidity vertical profiles of the 10-member ensemble as the large-scale reference profiles. We then enforce the WTG approximation over a range of τ or α (depending on the scheme used) values, and run a 5-member ensemble over a period of 250 days for each of the configurations, taking statistics every hour over the last 100 days. For each member in the ensembles, perturbations were made to the initial state of the model, resulting in a mix of wet and dry final states. In order to make it easier to obtain both wet- and dry-states of the multiple-equilibria regime, we perturbed the large-scale reference profile uniformly in the vertical by -0.05 K for another 5-member ensemble, and $+0.05$ K for a final 5-member ensemble respectively.

In order to showcase the difference between the RCE and WTG states, we implement a smooth transition from a pseudo-RCE state ($\alpha(t=0) = \tau(t=0) = \infty$) to a WTG state ($\alpha = \alpha_0$ or $\tau = \tau_0$), where α_0 and τ_0 are the final strength of the WTG approximation at $t = t_{\mathrm{wtg}}$. In all our experiments, we take $t_{\mathrm{wtg}} = 25$ days, which means that in our experimental runs the WTG implementations will reach maximum strength at 25 days from model startup.

4 Divergence in Model Behavior with different WTG Schemes under an Idealized Model Framework

Applying the WTG approximation to small-domain models with interactive radiative schemes results in multiple-equilibria (see Fig. 2i), with permanent wet and dry model states both being possible outcomes regardless of the WTG scheme. Results from the different WTG schemes are qualitatively similar to each other and to the results of Emanuel et al. (2014) using the MITgcm in single-column mode, but have significant quantitative differences. As the strength of the WTG adjustment increases, the model eventually enters an oscillatory regime where the model rapidly alternates between wet and dry states (see whiskers in Fig. 2, and daily-averaged time-series plots in Fig. S2). However, we note that the magnitude of these oscillations is very small in TGR simulations compared to when the DGW and SPC implementations are used.

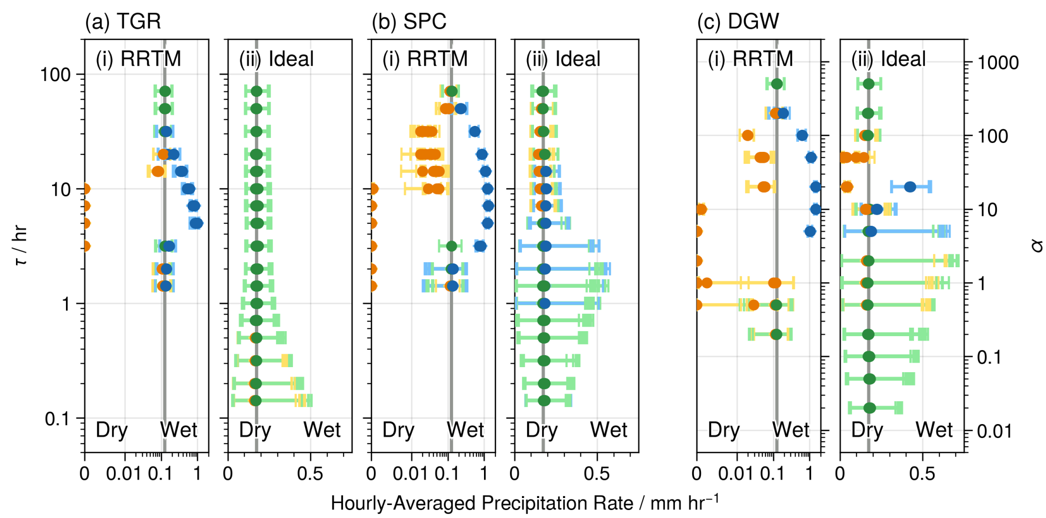

Figure 2. Domain-mean hourly-averaged precipitation rate P_{WTG} for the (a) Temperature Gradient Relaxation (TGR, Raymond and Zeng (2005)), (b) Spectral (SPC, Herman and Raymond (2014)) Weak Temperature Gradient and (c) Damped Gravity Wave (DGW, Kuang (2008a); Blossey et al. (2009)) implementations respectively, for the (i) RRTM radiation and (ii) idealized-radiative cooling schemes respectively. The gray-line denotes RCE time-averaged domain-mean hourly-averaged precipitation rate $\mu(P_{\mathrm{RCE}})$, dots represent the time-averaged mean for each ensemble member $\mu(P_{\mathrm{WTG}})$, while the whiskers denote the 5-th and 95-th percentiles of the hourly-averaged rates. Yellow indicates $\mu(P_{\mathrm{WTG}}) < 0.95\mu(P_{\mathrm{RCE}})$ for an individual ensemble member, blue when $\mu(P_{\mathrm{WTG}}) > 1.05\mu(P_{\mathrm{RCE}})$, and green otherwise.

Model behavior varies even more markedly between the different WTG schemes (Fig. 2ii) when the idealized-radiation framework described in Section 3 is used. In the DGW framework, while the multiple-equilibrium regime is greatly reduced compared to realistic-radiation simulations, it is still significant and leads into an oscillatory regime (see the timeseries of daily-averaged precipitation in Fig. S3), and the results found by Sessions et al. (2016). However in the SPC framework, the bifurcation between the wet- and dry-states of the multiple-equilibrium regime is reduced until it is almost indistinguishable from the RCE-mean (though the presence of yellow and blue dots in Fig. 2cii indicates that it is not entirely gone). A significant oscillatory regime still exists when the strength of the implementation is large ($\tau < 10$ hr). In the TGR framework the oscillatory regime does not even become significant until τ approaches values that are not physical (e.g. $\tau < 0.5$ hr).

We see that these differences in model behavior upon the implementation of different WTG schemes is larger in a simple model framework with idealized radiation (Fig. 2). The implementation of full interactive radiation serves to mask the differences in model behavior by amplifying the multiple-equilibria regime, similar to how fully-interactive radiation has been considered by many previous studies (e.g. Bretherton et al., 2005; Muller & Held, 2012; Coppin & Bony, 2015; Holloway & Woolnough, 2016; Wing et al., 2017; Pope et al., 2023) to be a key component of self-aggregated convection.

Since the contrast between WTG schemes is best shown in model frameworks with idealized radiation, the model results in the sections below are therefore limited to experimental setups with idealized radiation. Nonetheless, because the model results from the DGW and SPC implementations are qualitatively more similar to each other than between the DGW and TGR implementations across different radiation schemes, we believe that our discussions in Sections 5 and 6 would still be applicable to model frameworks with fully-interactive radiation.

5 Revisiting the different WTG schemes using a Vertical Mode Decomposition

We now seek to understand the differences between these implementations. Similar to Kuang (2008b); Herman and Raymond (2014), we decompose both the left- and right-hand-side components of Eq. 4 into linear combinations of the vertical modes G_j (see Eq. 6):

$$\omega' = \sum_{j=1}^{n} \omega_j G_j(z) \qquad\qquad \frac{\overline{p}T_v'}{\overline{T}^2} = \sum_{j=1}^{n} T_j G_j(z) \tag{8}$$

Noting that the equations in the DGW implementation solve not for ω', but for $\partial_{zz}\omega'$, we see that ω_j and T_j are related to each other as follows:

$$-\frac{\pi^2}{z_t^2}\sum_{j=1}^{n} j^2\omega_j G_j(z) = \partial_{zz}\omega' = \frac{k^2}{\alpha a_m}\frac{\overline{p}g^2}{R_d\overline{T}^2}T_v' = \frac{1}{\alpha}\cdot\frac{k^2g^2}{R_d a_m}\sum_{j=1}^{n} T_j G_j(z) \tag{9}$$

$$\begin{aligned} \therefore \omega_j &= -\frac{T_j}{j^2}\cdot\frac{1}{\alpha}\cdot\frac{z_t^2k^2g^2}{R_d a_m \pi^2} \\ &= -\frac{T_j}{j^2}\cdot\frac{c}{\alpha} \end{aligned} \tag{10}$$

where $c = \frac{z_t^2k^2g^2}{R_d a_m \pi^2}$, and since fluctuations in c depend only on z_t, which can be assumed to be constant compared to the range of α explored, we can assume that c is constant as well.

A similar analysis of the TGR implementation gives:

$$\sum_{j=1}^{n} w_j G_j(z) = w' = \frac{\theta'}{\tau\cdot\partial_z\overline{\theta}} = \frac{1}{\tau}\sum_{j=1}^{n}\theta_j G_j(z) \tag{11}$$

$$\therefore w_j = \theta_j\cdot\frac{1}{\tau} \tag{12}$$

Lastly, analysis of the SPC implementation gives (see Section 2.3):

$$w_j = \frac{\theta_j}{\tau_j} = \frac{\theta_j}{j}\cdot\frac{1}{\tau} \tag{13}$$

A comparison of Eqs. 10, 12 and 13 show that the higher-order modes in vertical velocity associated with the respective higher-order vertical modes of local buoyancy-temperature anomalies are different in the different WTG schemes. For a given buoyancy-temperature perturbation, the resulting higher-order modes in vertical velocity decrease in strength in order of (1) DGW, (2) SPC and (3) TGR respectively. Therefore, the vertical structure of vertical velocity will be different across the different WTG schemes, where profiles from the TGR implementation are likely to have stronger higher-order modes compared to the profiles from the DGW or SPC implementations, and this has been well-documented (Romps, 2012b; Daleu et al., 2015, see also Fig. S1).

6 Bringing the different WTG Schemes together using the Gross Moist Stability Framework

Previous studies have shown that the basic dynamics of convectively coupled tropical waves can largely be captured by models which contain the first two baroclinic modes of the vertical structure of the tropical atmosphere (e.g. Mapes, 2000; Majda & Shefter, 2001; Khouider & Majda, 2006; Haertel & Kiladis, 2004; Kuang, 2008b). Using the first two baroclinic modes and ignoring all higher-order terms, we analyze our vertical mode decomposition of the various WTG implementations in the context of the GMS framework. Following Raymond et al. (2009); Kuang (2011); Inoue and Back (2015, 2017) we define:

$$\mathrm{GMS} = \frac{\langle w \cdot \partial_z h \rangle}{\langle w \cdot \partial_z s \rangle} = \frac{\langle W_1 \cdot \partial_z h \rangle + \langle W_2 \cdot \partial_z h \rangle}{\langle W_1 \cdot \partial_z s \rangle + \langle W_2 \cdot \partial_z s \rangle} \tag{14}$$

where angle brackets represent vertical averages. This is the ratio of the lateral export of moist static energy h to the vertical export of dry static energy s. W_1 and W_2 are the first and second modes of vertical velocity. Taking idealized vertical profiles of the dry and moist static energies shown in Fig. 3, we see that Eq. 14 can be reduced to:

$$\mathrm{GMS} = \frac{\langle w \cdot \partial_z h \rangle}{\langle w \cdot \partial_z s \rangle} \approx \frac{\langle W_2 \cdot \partial_z h \rangle}{\langle W_1 \cdot \partial_z s \rangle} = \frac{w_2 \langle \sin(2\pi z/z_t) \cdot \partial_z h \rangle}{w_1 \langle \sin(\pi z/z_t) \cdot \partial_z s \rangle} \tag{15}$$

Thus, any change to the GMS is ultimately dominated by the relative strengths of the first two baroclinic modes. However, as we have discussed previously, the response of higher-order baroclinic modes to a given buoyancy perturbation is different across the WTG implementations. For example, because the SPC and TGR implementations result in stronger 2nd baroclinic modes, and thus stronger 2nd-order modes of vertical velocity, it would favor higher GMS magnitudes than the DGW implementation and thus larger magnitudes of export (or import) of moist static energy. This is in line with the characterization of GMS as a quantity that describes the (de)stabilization mechanisms of convective disturbances in the atmosphere (e.g. Raymond et al., 2009; Inoue & Back, 2015, 2017). We believe that the ratio $w_r = w_2/w_1$ therefore constrains how rapidly these convective disturbances are magnified/reduced.

As an example, we consider a moist environment with stronger-than-RCE deep convection. Such a moist and strongly-convecting environment will often have temperature profiles that are warmer in the upper troposphere and cooler in the lower troposphere. Assuming Rayleigh friction, a limited area warm anomaly aloft and an underlying cool anomaly will result in an adjustment circulation (in a non-rotating environment) that has ascent at upper levels and descent at lower levels, i.e., a circulation with positive second mode structure shown in Fig. 3a. As elaborated by Raymond et al. (2009); Inoue and Back (2015, 2017) and many other studies, this stratiform profile of convection tends

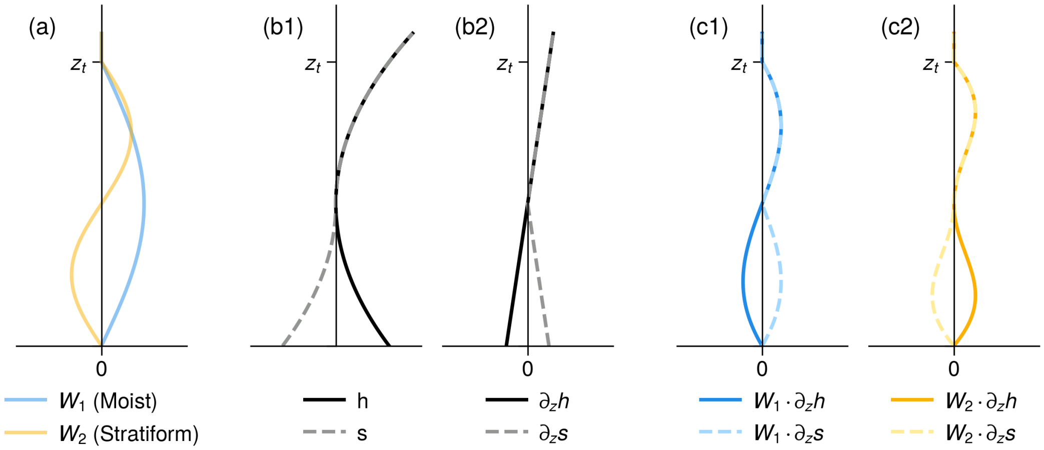

Figure 3. We plot an idealized profile of the (a) first two baroclinic modes of WTG-induced vertical velocity, (b) vertical profiles of (1) dry and moist static energy and (2) their vertical derivatives, and lastly (c) the product of the vertical derivatives of the static energies with the (1) first and (2) second vertical modes of vertical velocity. We see that the lateral export of moist and dry static energies are dominated by the 2nd and 1st baroclinic modes respectively.

to export GMS and return the domain-mean back to RCE. The greater the value w_r, the stronger this tendency. As the TGR implementation's greater emphasis on higher-order baroclinic modes naturally results in higher values of w_r, we see that in the idealized-radiation framework there is no visible bifurcation or multiple-equilibria (Fig. 2aii) when the TGR implementation is used. In contrast, higher-order baroclinic modes are weak in the DGW implementation, which results in a multiple-equilibria regime and a noticeable bifurcation in the resulting wet and dry states (Fig. 2cii).

We therefore hypothesize that the discrepancies in model behavior when different WTG schemes are used can be attributed to the differences in treatment of the baroclinic modes between these schemes. If we modify the TGR and SPC implementations such that the response strength of higher baroclinic modes is reduced, the multiple-equilibria regime may appear. To test this hypothesis, we modified the DGW and TGR implementations such that only the response of the first two baroclinic modes impact the system (note that in such a case, the form of the TGR and SPC implementations would be the same), and calculated the WTG-induced vertical velocities for the DGW and TGR implementations respectively to be:

$$\omega' = c_1 \omega_1 \sin\frac{\pi z}{z_t} + c_2 4\omega_2 \sin\frac{2\pi z}{z_t} \qquad\qquad w' = c_1 w_1 \sin\frac{\pi z}{z_t} + c_2 w_2 \sin\frac{2\pi z}{z_t} \tag{16}$$

where c_1 and c_2 vary vertical velocity associated with the first and second baroclinic modes to the first and second vertical modes of the temperature perturbation.

We vary different configurations of c_1 and c_2 as follows:

$$(c_1, c_2) = \begin{cases} 0 \leq c_1 \leq 1 & c_2 = 1 \\ 0 \leq c_2 \leq 1 & c_1 = 1 \end{cases} \tag{17}$$

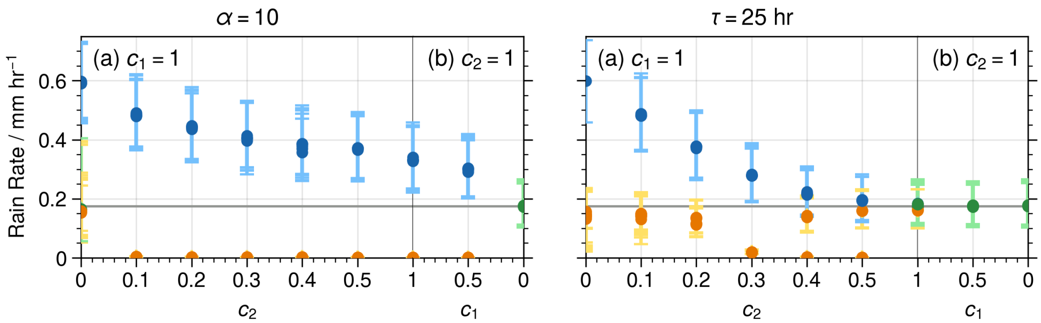

Figure 4. We show here how the strength of the bifurcation varies with the ratio of $c_r = c_2/c_1$ for the (a) DGW and (b) TGR implementations in experimental setups with idealized radiation. As c_r decreases, the bifurcation between the wet- and dry-states of the multiple-equilibria regime increases in magnitude.

Similar to Section 3.3, to obtain both wet- and dry-states of the multiple-equilibria regime, we perturbed the large-scale reference profiles, but this time by ± 0.1 K. We used the idealized radiation scheme of Pauluis and Garner (2006), and plot the results for $\alpha = 10$ and $\tau = 25$ hr in Fig. 4. As postulated above, the presence and strength of multiple-equilibria is indeed tied to the ratio of $c_r = c_2/c_1$, with smaller values of c_r resulting in stronger bifurcation into the wet and dry equilibrium states. When $c_1 = 0$, there is no bifurcation between wet and dry equilibrium states, nor any oscillatory behavior, even at much lower values of τ.

We also note the discrepancy when $c_2 = 0.5$, which is when the idealized TGR implementation is equivalent to the SPC implementation (if $n = 2$ in Eq. 6 of the SPC implementation, see Section 2.3). In Fig. 2 we see that the SPC implementation's multiple-equilibria regime is weaker than in Fig. 4 for an equivalent τ. This is presumably due to the effect of higher-order baroclinic modes beyond the 2nd-order. We are able to verify this by running a modified version of the SPC implementation where Eq. 14 is modified to:

$$w_j = \frac{\theta_j}{j^2} \cdot \frac{1}{\tau} \tag{18}$$

and our results (Fig. S4) show that the multiple-equilibria regime is now visible.

Lastly, in this paper we are focused on understanding the behaviors of different implementations of the WTG approximation under the assumption of Rayleigh damping. In observations, a warm anomaly aloft with an underlying cool anomaly are sometimes found to correspond to a more bottom-heavy convective mass flux (Raymond et al., 2014, 2015; Fuchs-Stone et al., 2020; Raymond & Fuchs-Stone, 2021), opposite to what is shown in Fig. 3a. Whether this discrepancy is due to the assumption of Rayleigh friction or the assumption of the WTG balance warrants additional study, but this is beyond the scope of our paper.

7 Conclusions

Implementing different WTG schemes results in different model behavior, and these differences become more prominent under a simplified framework with idealized radiation. A multiple-equilibria regime appears when the DGW implementation is used, with persistent wet and dry states. When the WTG approximation is enhanced more strongly, the model transitions into a regime that oscillates between these wet and dry states. However, when the TGR and SPC schemes are implemented the multiple-equilibria regime either weakens or vanishes, and the oscillatory behavior only appears in the TGR scheme when the relaxation occurs over unrealistically short timescales ($\tau \sim 0.1$ hr).

We have shown that these discrepancies can be attributed to their different treatments of higher-order baroclinic modes. Specifically, WTG schemes with stronger higher-order baroclinic modes reduce the likelihood of the multiple-equilibria and oscillatory regimes appearing. We can understand these differences in the GMS framework, specifically in reference to how Inoue and Back (2017) characterized GMS as a measure of feedback effects to convection. By approximating GMS as the ratio of export of moist static energy to that of dry static energy (Eq. 15, see also Raymond et al. (2009); Kuang (2011); Inoue and Back (2015)), we see that the choice of WTG scheme will play a significant role in the GMS of the system, particularly because the response of vertical velocity to buoyancy perturbations of the different baroclinic modes are treated differently.

As we first touched upon in our introduction, while some work has gone into quantifying the discrepancies in model results when different implementations are used (e.g. Romps, 2012a, 2012b; Daleu et al., 2015), less thought has been given to understanding why different implementations give rise to different results in the first place. We hope that this set of idealized model experiments begins to close the gap between quantifying and understanding the differences in model results when different WTG schemes are used.

8 Open Research

The climate model is built upon the System for Atmospheric Modelling v6.11.8 (Khairoutdinov & Randall, 2003). Our modified version of the source code for the model is available at `https://github.com/KuangLab-Harvard/SAM_SRCv6.11` (checkout the version 2.2.1) and is meant to replace the `SRC` folder. The Julia Language code that was used in setting up the model experiments, analyzing our results, and the notebooks used in producing our figures, available at Wong (2023b), and the raw data at Wong (2023a).

Acknowledgments

This research was supported by NSF grants AGS-1759255 and OISE-1743753. We thank Marat Khairoutdinov for making SAM available, and David Raymond and an anonymous reviewer for helpful comments. The Harvard Odyssey cluster provided the computing resources for this work.

References

Blossey, P. N., Bretherton, C. S., & Wyant, M. C. (2009, 3). Subtropical Low Cloud Response to a Warmer Climate in a Superparameterized Climate Model. Part II: Column Modeling with a Cloud Resolving Model. *Journal of Advances in Modeling Earth Systems*, *1*(3), n/a-n/a. doi: 10.3894/JAMES.2009.1.8

Bretherton, C. S., Blossey, P. N., & Khairoutdinov, M. (2005, 12). An Energy-Balance Analysis of Deep Convective Self-Aggregation above Uniform SST. *Journal of the Atmospheric Sciences*, *62*(12), 4273–4292. doi: 10.1175/JAS3614.1

Coppin, D., & Bony, S. (2015, 12). Physical mechanisms controlling the initiation of convective self-aggregation in a General Circulation Model. *Journal of Advances in Modeling Earth Systems*, *7*(4), 2060–2078. doi: 10.1002/2015MS000571

Daleu, C. L., Plant, R. S., Woolnough, S. J., Sessions, S., Herman, M. J., Sobel, A., ... van Ulft, L. (2015, 12). Intercomparison of methods of coupling between convection and large-scale circulation: 1. Comparison over uniform surface conditions. *Journal of Advances in Modeling Earth Systems*, *7*(4), 1576–1601. doi: 10.1002/2015MS000468

Daleu, C. L., Woolnough, S. J., & Plant, R. S. (2012, 12). Cloud-Resolving Model Simulations with One- and Two-Way Couplings via the Weak Temperature Gradient Approximation. *Journal of the Atmospheric Sciences*, *69*(12), 3683–3699. doi: 10.1175/JAS-D-12-058.1

Emanuel, K., Wing, A. A., & Vincent, E. M. (2014, 3). Radiative-convective instability. *Journal of Advances in Modeling Earth Systems*, *6*(1), 75–90. doi: 10.1002/2013MS000270

Fuchs-Stone, Z., Raymond, D. J., & Sentic, S. (2020, 6). OTREC2019: Convection Over the East Pacific and Southwest Caribbean. *Geophysical Research Letters*, *47*(11). doi: 10.1029/2020GL087564

Haertel, P. T., & Kiladis, G. N. (2004, 11). Dynamics of 2-Day Equatorial Waves. *Journal of the Atmospheric Sciences*, *61*(22), 2707–2721. doi: 10.1175/JAS3352.1

Herman, M. J., & Raymond, D. J. (2014, 12). WTG cloud modeling with spectral decomposition of heating. *Journal of Advances in Modeling Earth Systems*, *6*(4), 1121–1140. doi: 10.1002/2014MS000359

Holloway, C. E., & Woolnough, S. J. (2016, 3). The sensitivity of convective aggregation to diabatic processes in idealized radiative-convective equilibrium simulations. *Journal of Advances in Modeling Earth Systems*, *8*(1), 166–195. doi: 10.1002/2015MS000511

Inoue, K., & Back, L. E. (2015, 11). Gross Moist Stability Assessment during TOGA COARE: Various Interpretations of Gross Moist Stability. *Journal of the Atmospheric Sciences*, *72*(11), 4148–4166. doi: 10.1175/JAS-D-15-0092.1

Inoue, K., & Back, L. E. (2017, 6). Gross Moist Stability Analysis: Assessment of Satellite-Based Products in the GMS Plane. *Journal of the Atmospheric Sciences*, *74*(6), 1819–1837. doi: 10.1175/JAS-D-16-0218.1

Khairoutdinov, M. F., & Randall, D. A. (2003, 2). Cloud Resolving Modeling of the ARM Summer 1997 IOP: Model Formulation, Results, Uncertainties, and Sensitivities. *Journal of the Atmospheric Sciences*, *60*(4), 607–625. doi: 10.1175/1520-0469(2003)060⟨0607:CRMOTA⟩2.0.CO;2

Khouider, B., & Majda, A. J. (2006, 4). A Simple Multicloud Parameterization for Convectively Coupled Tropical Waves. Part I: Linear Analysis. *Journal of the Atmospheric Sciences*, *63*(4), 1308–1323. doi: 10.1175/JAS3677.1

Kuang, Z. (2008a, 2). Modeling the Interaction between Cumulus Convection and Linear Gravity Waves Using a Limited-Domain Cloud System–Resolving Model. *Journal of the Atmospheric Sciences*, *65*(2), 576–591. doi: 10.1175/2007JAS2399.1

Kuang, Z. (2008b, 3). A Moisture-Stratiform Instability for Convectively Coupled Waves. *Journal of the Atmospheric Sciences*, *65*(3), 834–854. doi: 10.1175/2007JAS2444.1

Kuang, Z. (2011, 1). The Wavelength Dependence of the Gross Moist Stability and the Scale Selection in the Instability of Column-Integrated Moist Static Energy. *Journal of the Atmospheric Sciences*, *68*(1), 61–74. doi: 10.1175/2010JAS3591.1

Majda, A. J., & Shefter, M. G. (2001, 6). Models for Stratiform Instability and Convectively Coupled Waves. *Journal of the Atmospheric Sciences*, *58*(12), 1567–1584. doi: 10.1175/1520-0469(2001)058⟨1567:MFSIAC⟩2.0.CO;2

Mapes, B. E. (2000, 5). Convective Inhibition, Subgrid-Scale Triggering Energy, and Stratiform Instability in a Toy Tropical Wave Model. *Journal of the Atmospheric Sciences*, *57*(10), 1515–1535. doi: 10.1175/1520-0469(2000)057⟨1515:CISSTE⟩2.0.CO;2

Mlawer, E. J., Taubman, S. J., Brown, P. D., Iacono, M. J., & Clough, S. A. (1997, 7). Radiative transfer for inhomogeneous atmospheres: RRTM, a validated correlated-k model for the longwave. *Journal of Geophysical Research: Atmospheres*, *102*(D14), 16663–16682. doi: 10.1029/97JD00237

Muller, C. J., & Held, I. M. (2012, 8). Detailed Investigation of the Self-Aggregation of Convection in Cloud-Resolving Simulations. *Journal of the Atmospheric Sciences*, *69*(8), 2551–2565. doi: 10.1175/JAS-D-11-0257.1

Pauluis, O., & Garner, S. (2006, 7). Sensitivity of Radiative–Convective Equilibrium Simulations to Horizontal Resolution. *Journal of the Atmospheric Sciences*, *63*(7), 1910–1923. doi: 10.1175/JAS3705.1

Pope, K. N., Holloway, C. E., Jones, T. R., & Stein, T. H. M. (2023, 2). Radiation, Clouds, and Self-Aggregation in RCEMIP Simulations. *Journal of Advances in Modeling Earth Systems*, *15*(2). doi: 10.1029/2022MS003317

Raymond, D. J., & Fuchs-Stone, Z. (2021, 2). Emergent Properties of Convection in OTREC and PREDICT. *Journal of Geophysical Research: Atmospheres*, *126*(4). doi: 10.1029/2020JD033585

Raymond, D. J., Fuchs-Stone, Z., Gjorgjievska, S., & Sessions, S. (2015, 9). Balanced dynamics and convection in the tropical troposphere. *Journal of Advances in Modeling Earth Systems*, *7*(3), 1093–1116. doi: 10.1002/2015MS000467

Raymond, D. J., Gjorgjievska, S., Sessions, S., & Fuchs-Stone, Z. (2014, 3). Tropical cyclogenesis and mid-level vorticity. *Australian Meteorological and Oceanographic Journal*, *64*(1), 11–25. doi: 10.22499/2.6401.003

Raymond, D. J., Sessions, S. L., Sobel, A. H., & Fuchs, Z. (2009, 3). The Mechanics of Gross Moist Stability. *Journal of Advances in Modeling Earth Systems*, *1*(3), n/a-n/a. doi: 10.3894/JAMES.2009.1.9

Raymond, D. J., & Zeng, X. (2005, 4). Modelling tropical atmospheric convection in the context of the weak temperature gradient approximation. *Quarterly Journal of the Royal Meteorological Society*, *131*(608), 1301–1320. doi: 10.1256/qj.03.97

Romps, D. M. (2012a, 9). Numerical Tests of the Weak Pressure Gradient Approximation. *Journal of the Atmospheric Sciences*, *69*(9), 2846–2856. doi: 10.1175/JAS-D-11-0337.1

Romps, D. M. (2012b, 9). Weak Pressure Gradient Approximation and Its Analytical Solutions. *Journal of the Atmospheric Sciences*, *69*(9), 2835–2845. doi: 10.1175/JAS-D-11-0336.1

Sessions, S. L., Sentić, S., & Herman, M. J. (2016, 3). The role of radiation in organizing convection in weak temperature gradient simulations. *Journal of Advances in Modeling Earth Systems*, *8*(1), 244–271. doi: 10.1002/2015MS000587

Sessions, S. L., Sugaya, S., Raymond, D. J., & Sobel, A. H. (2010, 6). Multiple equilibria in a cloud-resolving model using the weak temperature gradient approximation. *Journal of Geophysical Research*, *115*(D12), D12110. doi: 10.1029/2009JD013376

Sobel, A. H., Bellon, G., & Bacmeister, J. (2007, 11). Multiple equilibria in a single-column model of the tropical atmosphere. *Geophysical Research Letters*, *34*(22), L22804. doi: 10.1029/2007GL031320

Sobel, A. H., & Bretherton, C. S. (2000, 12). Modeling Tropical Precipitation in a Single Column. *Journal of Climate*, *13*(24), 4378–4392. doi: 10.1175/1520-0442(2000)013⟨4378:MTPIAS⟩2.0.CO;2

Wing, A. A., Emanuel, K., Holloway, C. E., & Muller, C. (2017, 11). Convective Self-Aggregation in Numerical Simulations: A Review. *Surveys in Geophysics*, *38*(6), 1173–1197. doi: 10.1007/s10712-017-9408-4

Wong, N. (2023a). *The Effect of Different Implementations of the Weak Temperature Gradient Approximation in Cloud Resolving Models (v3) [Dataset].* Harvard Dataverse. Retrieved from `https://doi.org/10.7910/DVN/YPXNPG` doi: 10.7910/DVN/YPXNPG

Wong, N. (2023b, 11). *natgeo-wong/2023GL104350 (v0.3) [Software].* Zenodo. Retrieved from `https://doi.org/10.5281/zenodo.10199461` doi: 10.5281/zenodo.10199461

Figure 1.

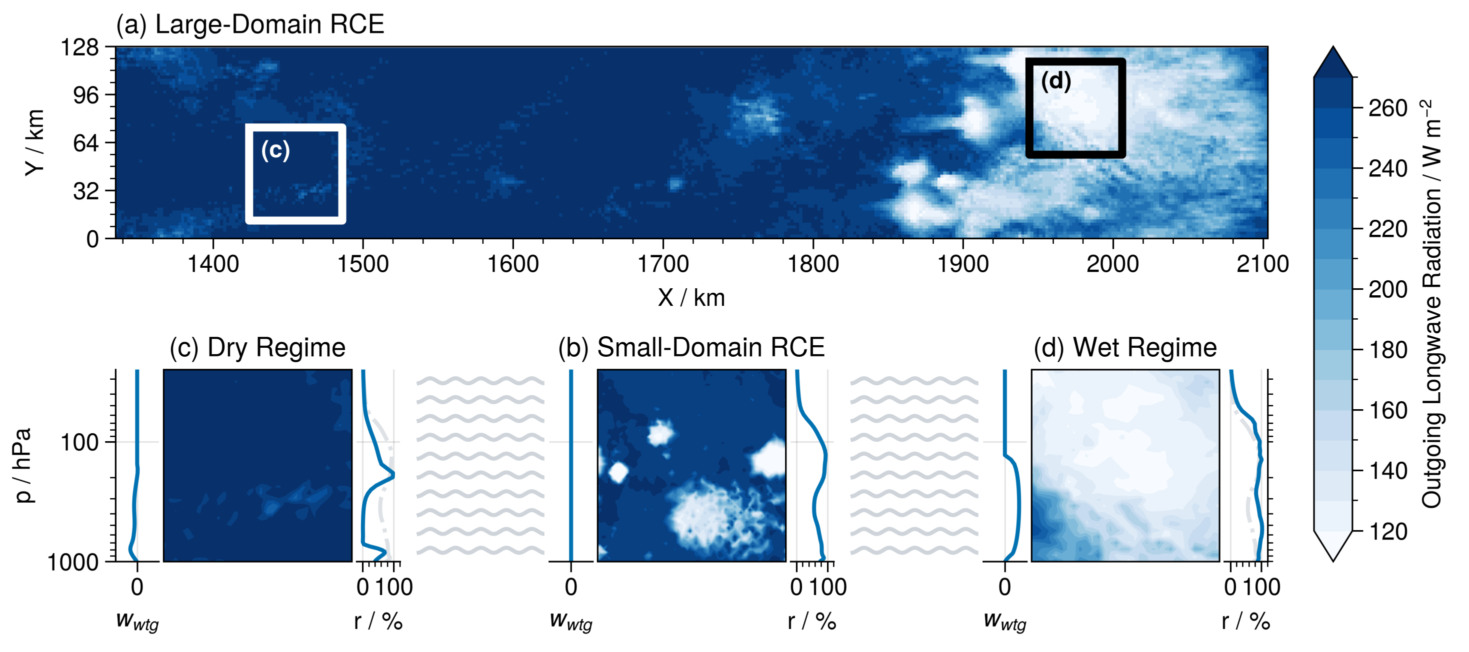

(a) Large-Domain RCE
Y / km
128
96
64
32
0
(c)
(d)
1400
1500
1600
1700
1800
1900
2000
2100
X / km
Outgoing Longwave Radiation / W m^{-2}
260
240
220
200
180
160
140
120
(c) Dry Regime
(b) Small-Domain RCE
(d) Wet Regime
p / hPa
100
1000
0
w_{wtg}
0 100
r / %

Figure 2.

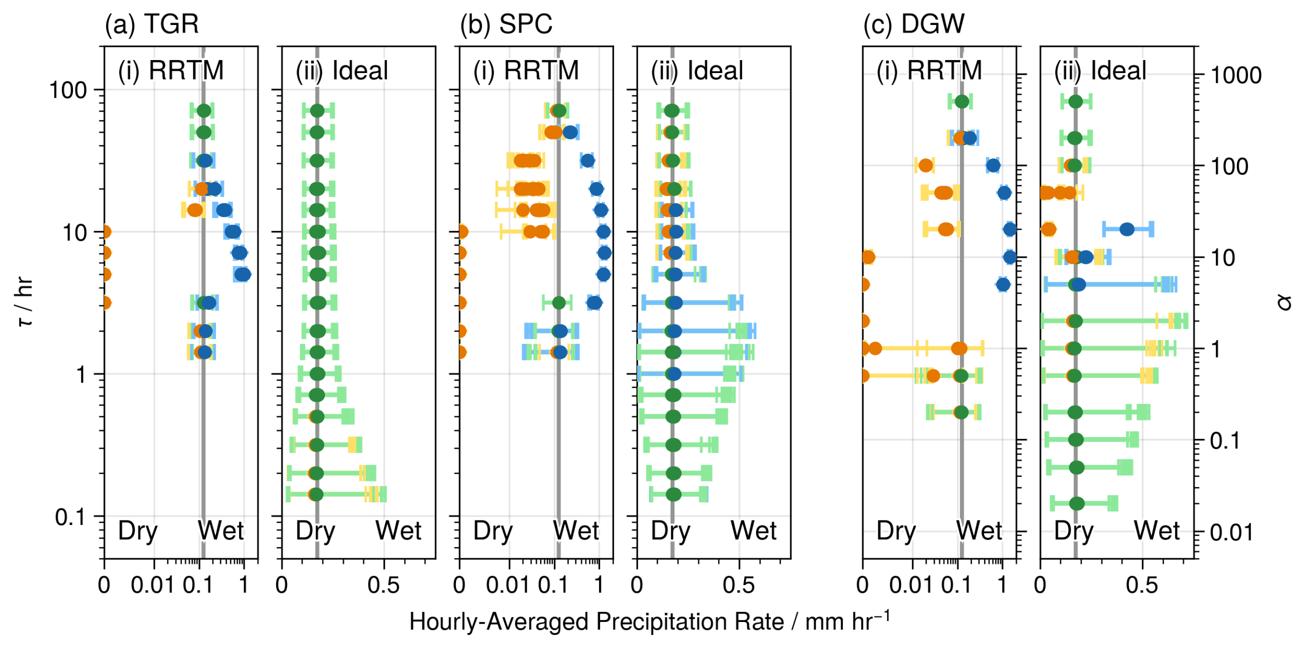

(a) TGR
(b) SPC
(c) DGW
(i) RRTM
(ii) Ideal
(i) RRTM
(ii) Ideal
(i) RRTM
(ii) Ideal
Dry
Wet
τ / hr
α
100
10
1
0.1
1000
100
10
1
0.1
0.01
0
0.01
0.1
1
0
0.5
Hourly-Averaged Precipitation Rate / mm hr^{-1}

Figure 3.

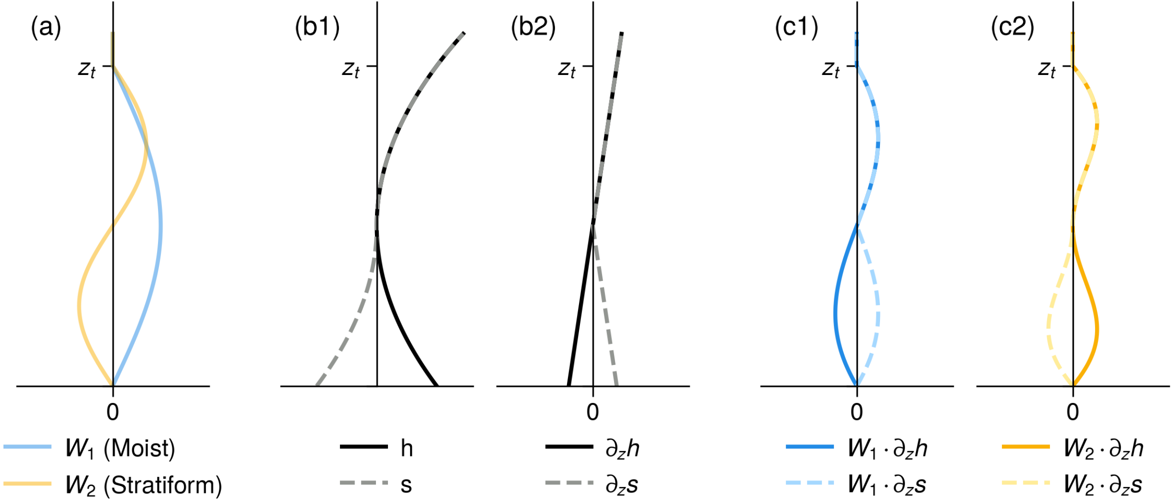

(a)
(b1)
(b2)
(c1)
(c2)
z_t
0
W_1 (Moist)
W_2 (Stratiform)
h
s
$\partial_z h$
$\partial_z s$
$W_1 \cdot \partial_z h$
$W_1 \cdot \partial_z s$
$W_2 \cdot \partial_z h$
$W_2 \cdot \partial_z s$

Figure 4.

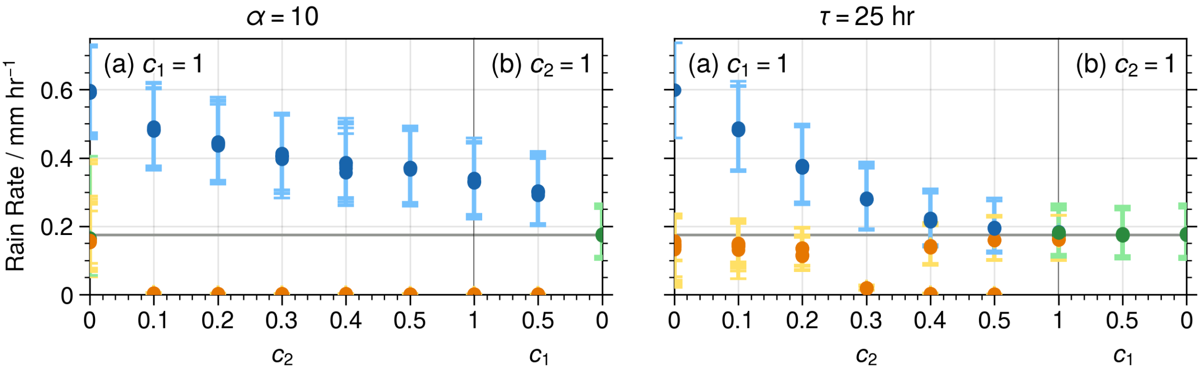

α = 10
τ = 25 hr
(a) c1 = 1
(b) c2 = 1
Rain Rate / mm hr−1
0
0.2
0.4
0.6
0
0.1
0.2
0.3
0.4
0.5
1
0.5
0
c2
c1